Supporting Information:
Chemical characterization, source, and SOA production of intermediate volatile organic compounds during haze episodes in North China

Text S1. Data preparation and factor determination of the PMF model

In the initial operation, carbonaceous components (SOC, POC, and EC); all-metal elements (Na, Mg, Al, Fe, V, Cr, Mn, Ni, Cu, Zn, As, Cd, and Pb); water-soluble ions (Na^+, K^+, Ca^{2+}, Mg^{2+}, Cl^-, NO_3^-, SO_4^{2-}, and NH_4^+); and non-polar (nC_{31}-nC_{34}) and polar compounds (LEV, MAN, C16A, and C18A) determined in Section 2.2 were input into the PMF model. Species with high noise and poor fitting, such as Na, Na^+, Ca^{2+}, Mg^{2+}, V, Zn, and Pb, were removed after random operation. Meanwhile, the $PM_{2.5}$ concentration was also included and set as weak to reduce its uncertainty in the model. Finally, 32 chemical components were inputted into the PMF model, including $PM_{2.5}$, SOC, POC, EC, Cl^-, NO_3^-, SO_4^{2-}, NH_4^+, K^+, Mg, Al, Fe, Mn, Cr, Ni, Cu, As, Cd, C_{31}, C_{32}, C_{33}, C_{34}, Fluoranthene (Fluo), Pyrene (Pyr), Benzo[a]anthracene (BaA), Chrysene (Chry), $PAHs_{252}$ (Benzo[b,k]fluorathene, Benzo[a, e]pyrene), $PAHs_{276}$ (IncdP and BghiP), Mannan (Man), Levoglucan (Lev), Hexadecanoic acid (C_{16}A), and Octadecanoic acid (C_{18}A). PAHs (Fluo Pyr, BaA, Chry, $PAHs_{252}$, $PAHs_{276}$) with low volatility and reactivity were selected in the PMF model to ensure the accuracy of source apportionment results. Among them, EC, K+, Mg, Ni, Cu, and As were set to be weak.

Nine factors were determined by the PMF model. The factor profiles are shown in Figure S2. The first factor (F1) was identified as an SOA source with a high proportion of SOC in F1, which was 76.4%. The secondary source (F2) was identified with high SO_4^{2-}, NO_3^-, and NH_4^+ concentrations accounting for 50.3%, 53.2%, and 43.8% in F2, respectively [1-3]. Factor (F3) presented high loading of Mg, Al, and Fe, which were mainly emitted from dust sources [4]. Factor (F4) was defined as the industry source owing to the high abundance of Cr and Ni, accounting for 75.0% and 83.1% in F4, respectively. Factor (F5) was mostly loaded by Cl-, As, Cd, and moderately loaded by POC and EC, which were mainly emitted from coal combustion [3, 5, 6]. The factor 6 (F6) featured a high abundance of C_{31}-C_{34}, and high-ring $PAHs_{276}$ (IncdP and BghiP) were assigned as gasoline vehicle sources [7-9]. The higher proportion of four-ring PAHs such as Fluo, Pyr, BaA, and Chry compared to five-ring/six-ring ($PAHs_{252}$ and $PAHs_{276}$) in F7 was defined as a diesel vehicle source [7, 8]. Factor F8 was interpreted as biomass burning since it featured high Lev and Man explained variances [10, 11]. Factor (F9), characterized by high C_{16}A and C_{18}A, was identified as a cooking source [12, 13].

The reasonable result was selected based on changes in the Q/Qexp value, source profiles, and bootstrap (BS) and displacement (DISP) analyses. The error analysis results of the PMF model are listed in Table S1. Minimizing the objective function Q in the PMF model obtains reasonable factor contributions and profiles. A series of effective tests was conducted to determine the optimal number of source factors, in which the number of factors ranged from 5 to 11. It is expected that additional factors will gradually decrease Q/Qexp. There was

a large decrease in Q/Qexp from six factors to eight factors (8.44%). The minimum value of Q/Qexp was obtained as 10-factor. However, when the number of factors increased up to 10 or larger, this separated the meaningless sources. In addition, for the eight-factor model, we found an 85% mapping of bootstrapping (BS) factors to base factors. However, for the nine-factor model, the BS factors were mapped over 95% for all factors, and no factor swapped with displacement (DISP) for dQmax = 4. Thus, nine factors were chosen as the most reasonable source profiles for PMF.

Text S2. Estimation of SOA mass yields and OH reaction rate constants for speciated IVOCs and un-speciated IVOCs UCM bins.

The selection of SOA yield in this study is when the OA concentration is 9 $\mu g \cdot cm^{-3}$ due to the lack of OA concentrations in the atmospheric environment, which is the most conservative estimation for SOA yields. Based on the simulation of the smoke box experiments, the SOA yields of C_9-C_{17} were from Zhao et al. [14] under high-NOx conditions. The SOA yields of C_{18}-C_{22} were assumed, adding C with a 10% increase in SOA yield from Aumount et al. [15]. The SOA yields of C_{18}-C_{22} are listed in Table S2. The SOA yields of naphthalene, methylnaphthalenes, and phenanthrene (1-Nap, 2-Nap, C2-Nap, and Phe) in PAHs came from Chan et al. [16]. The SOA yields of other PAHs were assumed to be similar to that of Phe, as shown in Table S2.

In addition, the SOA yields of un-speciated *b*-alkanes, cyclic-alkanes, and oxygenated compounds in IVOC bins were evaluated with the corresponding substitutes and selected according to the retention time of the known compound-*n*-alkane in each bin (Table S3). The SOA yields of *b*-alkanes in the Bn are represented by *n*-alkanes with a carbon chain number of (n-2). For example, the SOA yield of *b*-alkanes in B_{12} was represented by that of nC_{10}. This is due to the fact that *b*-alkanes are mainly composed of isomers with less than five carbons in the side chain, which corresponds to the Kovata retention index, and the retention time in gas chromatography is similar to that of linear isomers. The *b*-alkanes in B_{17} include C1-hexadecane, C_2-hexadecane, C_3-hexadecane, and C_4-pentadecane. As the number of branches increases, the decomposition rate of alkoxy groups increases, so nC_{15} is selected as a substitute for B_{17}. Moreover, *n*-alkanes (*n*-Cn) are used as substitutes for cyclic-alkanes (cyclic-Cn), which can be relatively conservative for estimating the SOA yields of cyclic-alkanes in the interval Bn [14, 17]. The retention time of the oxidation of IVOC UCM (oxygenated UCM) in the interval Bn is shorter than its hydrocarbon, and the distribution interval number differs from one to three. Therefore, *n*-alkanes with Cn-3 carbons are used as substitutes to estimate the SOA yield of oxygen-containing compounds in the interval Bn. Finally, the SOA yields of *n*-alkanes, PAHs, *b*-alkanes, cyclic-alkanes, and oxygenated UCM, the corresponding OH rate constants are from Zhao et al. [14, 17], as shown in Tables S2 and S3.

Table S1. BS Mapping of the nine factors.

	SOA source	SNA source	Dust source	Industry source	Coal combustion	Gasoline vehicle	Diesel vehicle	Biomass burning	Cooking source	Unmapped
Factor 1	100	0	0	0	0	0	0	0	0	0
Factor 2	0	95	0	0	0	4	1	0	0	0
Factor 3	0	0	100	0	0	0	0	0	0	0
Factor 4	1	0	0	98	0	0	0	1	0	0
Factor 5	1	0	0	0	95	2	2	0	0	0
Factor 6	0	0	0	0	0	100	0	0	0	0

Factor 7	0	0	0	0	0	0	100	0	0	0
Factor 8	0	1	1	0	1	1	0	96	0	0
Factor 9	0	0	0	0	0	0	0	0	100	0

DISP diagnostics: The DISP diagnostics of nine factors' results showed the Largest decrease in Q:0; % dQ:0; swaps by factor:0. The results show that there is no exchange among DISP diagnostics, and there is factor exchange among individual sources (BS>95) in the base run results of the model, and there is a certain degree of factor mixing, but it is within the acceptable range [18].

Table S2. SOA yields and OH rate constant of speciated IVOCs.

Compound	OH rate constant	SOA Yield
nC_9		0.01
nC_{10}		0.02
nC_{11}		0.05
nC_{12}	1.32E-11	0.09
nC_{13}	1.52E-11	0.21
nC_{14}	1.68E-11	0.28
nC_{15}	1.82E-11	0.34
nC_{16}	1.96E-11	0.38
nC_{17}	2.10E-11	0.42
nC_{18}	2.24E-11	0.46
nC_{19}	2.38E-11	0.51
nC_{20}	2.52E-11	0.56
nC_{21}	2.67E-11	0.62
nC_{22}	2.81E-11	0.68
Nap	2.3E-11	0.21
1-Nap	4.86E-11	0.38
2-Nap	4.09E-11	0.33
C_2-Nap	6.0E-11	0.31
Ace	8.0E-11	0.31
Acy	1.24E-11	0.31
Flu	1.6E-11	0.31
Phe	3.2E-11	0.31
Ant	1.78E-11	0.31
Fluo	3.3E-11	0.31
Pyr	5.6E-11	0.31

Table S3. SOA yields and OH rate constant of un-speciated IVOCs.

Bin	OH rate constant	Surrogate compound (n-alkane) for IVOC UCM		
		b-alkane IVOC UCM	Cyclic IVOC UCM	Oxygenated IVOC UCM
B_{12}	1.32E-11	C_{10}	C_{12}	C_9
B_{13}	1.52E-11	C_{11}	C_{12}	C_{10}
B_{14}	1.68E-11	C_{12}	C_{13}	C_{11}
B_{15}	1.82E-11	C_{13}	C_{14}	C_{12}
B_{16}	1.96E-11	C_{14}	C_{15}	C_{13}
B_{17}	2.10E-11	C_{15}	C_{16}	C_{14}
B_{18}	2.24E-11	C_{16}	C_{17}	C_{15}
B_{19}	2.38E-11	C_{17}	C_{18}	C_{16}
B_{20}	2.52E-11	C_{18}	C_{19}	C_{17}

B_{21}	2.67E-11	C_{19}	C_{20}	C_{18}
B_{22}	2.81E-11	C_{20}	C_{21}	C_{19}

Table S4. The detection limit and recovery rates of nC12-nC22 and PAHs by TD-GC/MS.

Species	Detection limit	Recovery rate	Species	Detection limit	Recovery rate
nC12	51.0ppb	-	Nap (d8-Nap)	35.7ppb	120.5±27%
nC13	49.1ppb	-	Acy (d10-Acy)	42.2ppb	80.1±7.8%
nC14	39.5ppb	-	Ace	32.2ppb	-
nC15	58.1ppb	-	Flu	20.8ppb	-
nC16(d34-nC16)	22.2ppb	100.2±31.9%	Phe (d10-Phe)	24.4ppb	73.2±7.1%
nC17	37.9ppb	-	Ant	43.1ppb	-
nC18	39.8ppb	-	Fluo	32.0ppb	-
nC19	44.4ppb	-	Pyr	63.4ppb	-
nC20	45.5ppb	-	1-Nap	35.8ppb	-
nC21	70.0ppb	-	2-Nap	36.7ppb	-
nC22	73.6ppb	-	2,6-Nap	10.1ppb	-

Table S5. Components characteristic of IVOCs during different pollution stages.

Haze stages	IVOCs	*n*-alkanes	PAHs	*b*-alkanes	R-UCM
LP1-1	43.8±9.0	4.0±0.9	1.4±0.4	11.9±5.1	22.4±8.4
		(11.2±3.5%)	(3.9±1.0%)	(28.9±3.6%)	(56.0±4.6%)
HP1-1	49.6±15.2	3.7±1.3	1.5±0.4	11.9±3.9	32.4±11.1
		(7.6±1.6%)	(3.1±0.7%)	(24.1±3.9%)	(65.1±6.0%)
LP1-2	40.5±9.7	2.6±0.8	1.4±0.4	8.2±2.8	22.3±10.2
		(8.2±2.0%)	(4.4±1.3%)	(24.8±4.1%)	(62.6±7.2%)
HP2-1	49.4±12.5	4.9±1.3	2.3±0.4	12.9±2.9	29.1±8.0
		(10.0±1.1%)	(4.9±1.1%)	(26.5±1.6%)	(58.6±3.6%)
LP2-1	30.7±8.0	2.4±0.8	1.7±0.5	7.0±2.1	19.4±4.9
		(7.9±1.3%)	(5.5±0.9%)	(22.9±1.6%)	(63.7±3.7%)
HP2-2	46.2±5.7	4.1±0.4	2.5±0.2	10.3±1.4	29.1±4.7
		(9.0±1.2%)	(5.6±0.7%)	(22.4±2.0%)	(63.0±3.6%)

Figures：

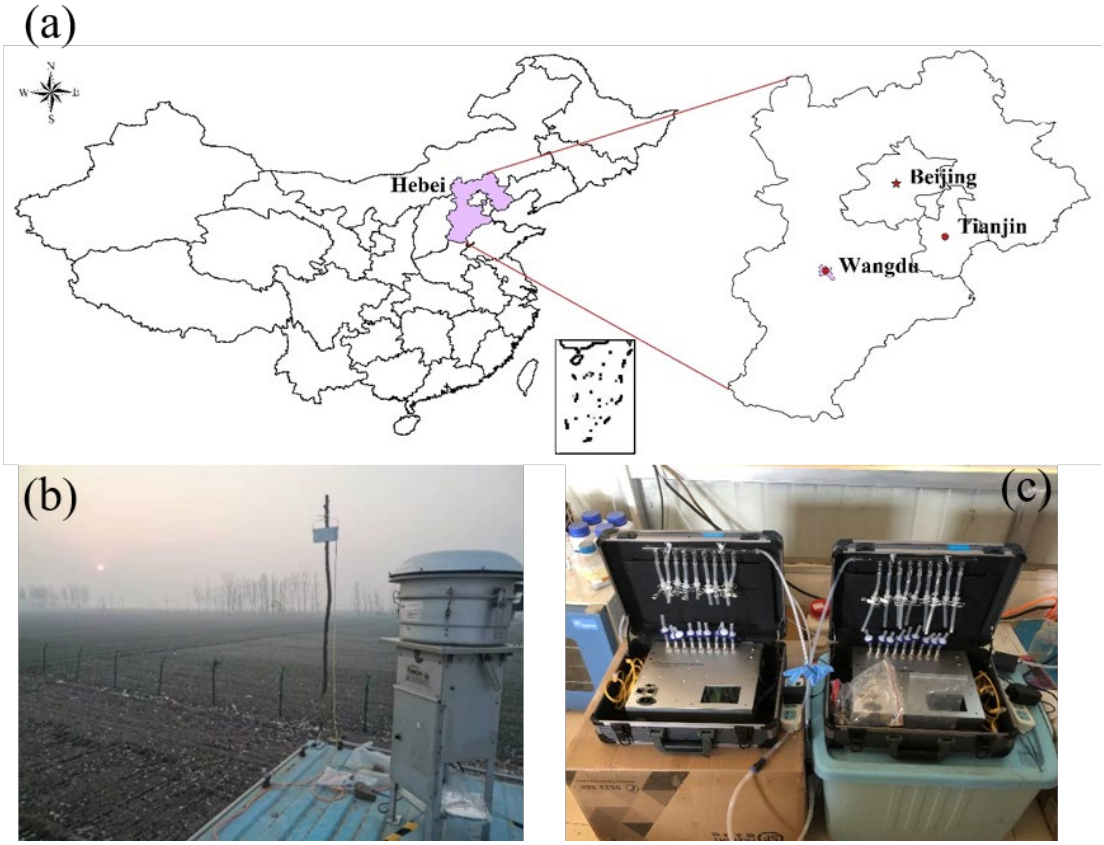

Figure S1. (a) Sampling site in Wangdu Country, Hebei Province, North China; (b) $PM_{2.5}$ sampling instrument; (c) IVOC sampling instrument.

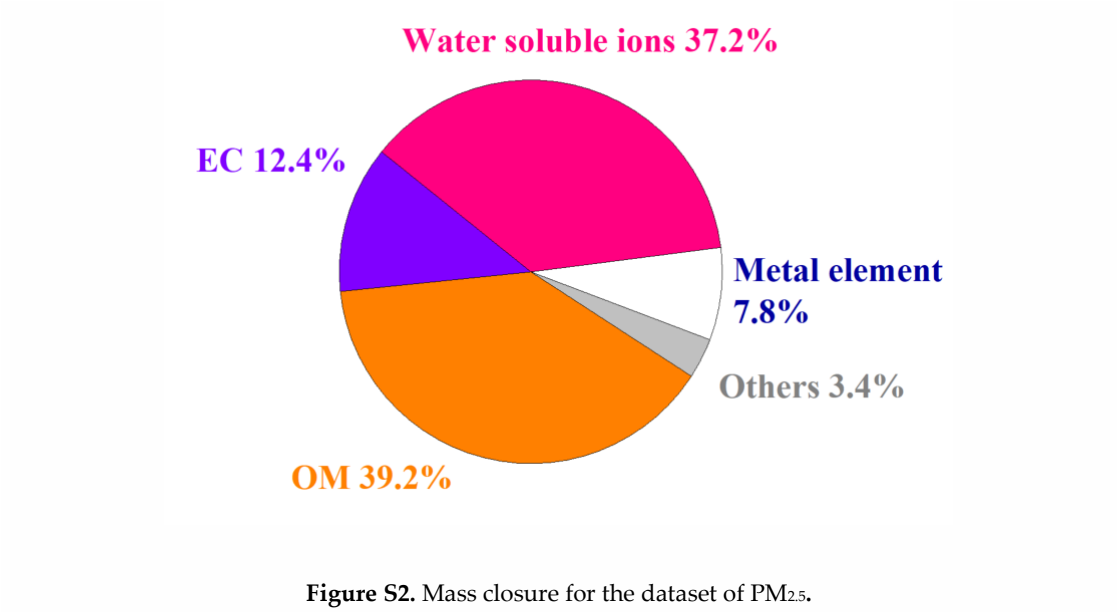

Figure S2. Mass closure for the dataset of $PM_{2.5}$.

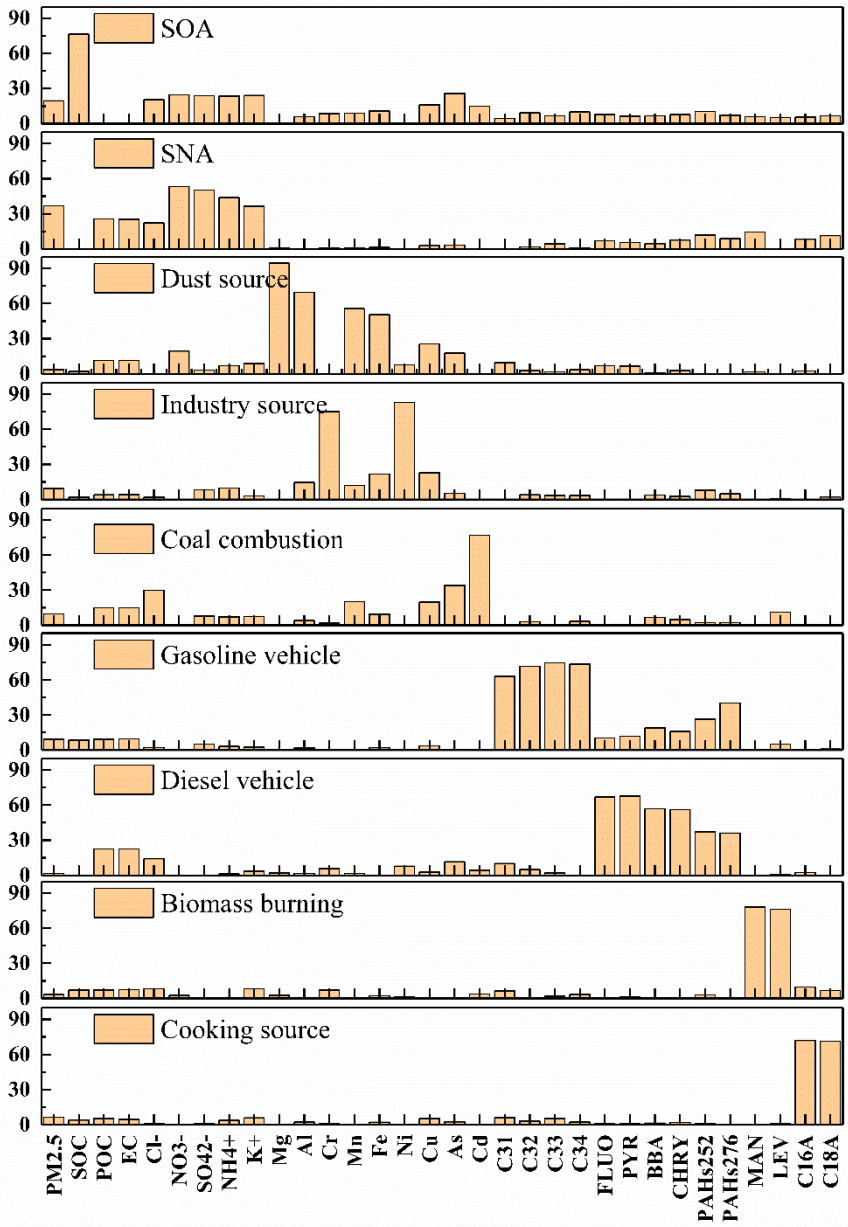

Figure S3. Factor profiles of $PM_{2.5}$ source apportionment based on the PMF model.

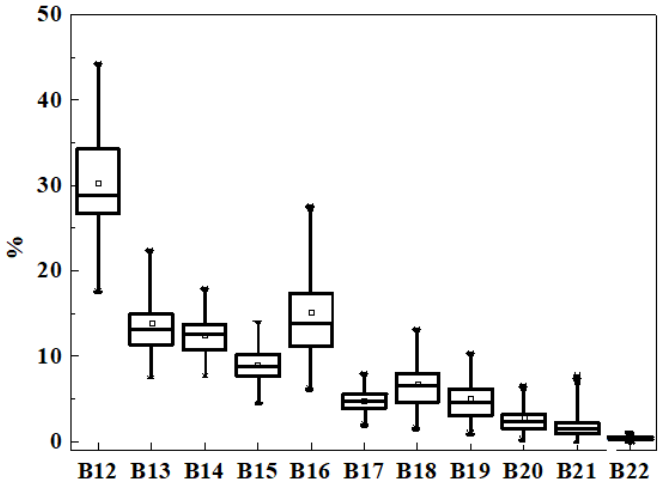

Figure S4. The ratio of Bn in IVOCs during the two haze episodes.

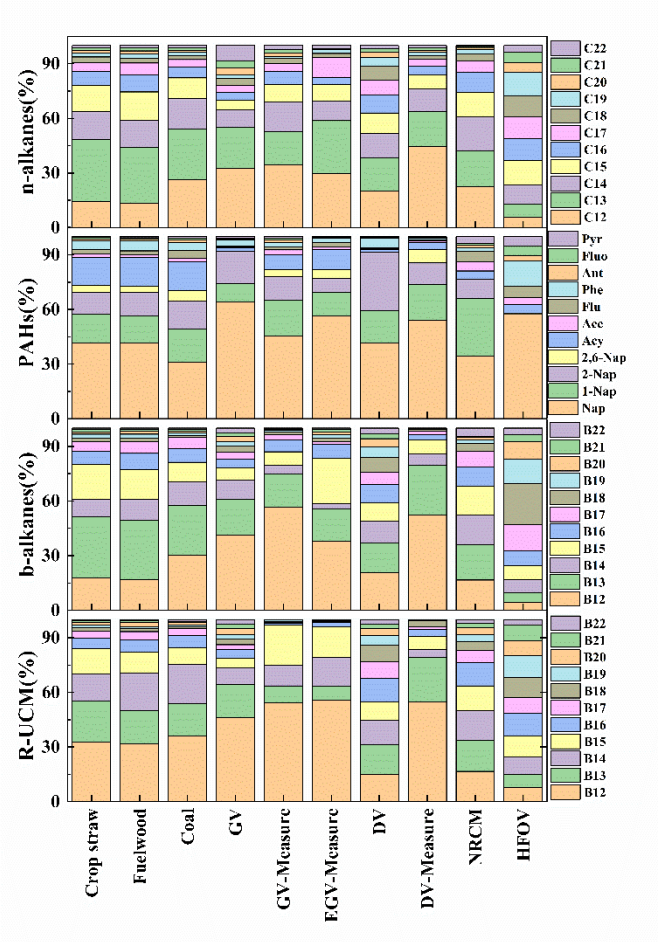

Figure S5. Component characteristics of IVOCs of various emission sources (GV: gasoline vehicle, GV-Measure: un-published gasoline vehicle from our research groups, EGV: ethanol–gasoline vehicle, DV: diesel vehicle, NRCM: no-road construction machinery; HFOV: heavy fuel oil vessel [19].)

References

1. Gao, J.; Peng, X.; Chen, G.; Xu, J.; Shi, L.; Zhang, Y.; Feng, Y. Insights into the chemical characterization and sources of PM2.5 in Beijing at a 1-h time resolution. *Sci. Total Environ.* **2016**. *542*, 162-171.

2. Shi, L.; Xu, J.; Peng, X.; Xiao, M.; Chen, K.; Tian, Z.; Guan, B.; Feng, C.; Yu, F.; Nenes, A.; et al. PH of aerosols in a polluted atmosphere: source contributions to highly acidic aerosol. *Environ. Sci. Technol.* **2017**. 51, 4289-4296.
3. Liu, Y.; Wang, A.; Cao, Y.; Yang, X.; Zhang, L.; Luan, X.; Lyu, D.; Hansen, A.D.A.; Liu, X.; Zheng, M. Impacts of COVID-19 on black carbon in two representative regions in China: Insights based on online measurement in Beijing and Tibet. *Geophys. Res. Lett.* **2021**. 48, e2021GL092770.
4. Shen, Z.; Sun, J.; Cao, J.; Zhang, M.; Zhang, Q.; Lei, L.; Gao J.; Huang, J.; Liu, X.; Huang, Y.; et al. Chemical profiles of urban fugitive dust PM2. 5 samples in Northern Chinese cities. *Sci. Total Environ*. **2016**. 569, 619-626.
5. Dai, L.; Liu, S.; Bi, H.; Wu, H.; Liang, N.; Zhang, F.; Feng, C.; Hopke, P.K. Dispersion normalized PMF provides insights into the significant changes in source contributions to PM2. 5 after the COVID-19 outbreak. *Environ. Sci. Technol*. **2020**. 54, 9917-9927.
6. Vejahati, F.; Xu, H.; Gupta, R. Trace elements in coal: Associations with coal and minerals and their behavior during coal utilization - A review. *Fuel*. **2010**. 89, 904-911.
7. Lv, L.; Chen, J.; Han, Y.; Cui, M.; Wei, P.; Zheng, M.; Hu, N. High-time-resolution PM2. 5 source apportionment based on multi-model with organic tracers in Beijing during haze episodes. *Sci. Total Environ*. **2021**. 772, 144766.
8. Perrone, M.G.; Carbone, C.; Faedo, D.; Ferrero, C.; Maggioni, A.; Sangiorgi, G.; Bolzacchini, E. Exhaust emissions of polycyclic aromatic hydrocarbons, n-alkanes and phenols from vehicles coming within different European classes. *Atmos. Environ*. **2014**. 82, 391-400.
9. Javed, W.; Iakovides, M.; Garaga, R.; Stephanou, E.G.; Kota, S.H.; Ying, Q.; Wolfson, J.M.; Koutrakis, P.; Guo, B. Source apportionment of organic pollutants in fine and coarse atmospheric particles in Doha, Qatar. *J. Air Waste Manage. Assoc*. **2019**. 1277-1292.
10. Wang, Q.; Huang, H.; Zhang, T.; Zhang, Y.; Feng, M.; Yuan, B.; Wu, D.; Lau, H.; Yu, Z; Organic tracer-based source analysis of PM2. 5 organic and elemental carbon: A case study at Dongguan in the Pearl River Delta, China. *Atmos. Environ*. **2015**. 118, 164-175.
11. Wang, Q.; Huang, X.H.H.; Tam, F.C.V.; Zhang, X.; Liu, M.; Yeung, C.; Feng, M.; Cheng, Y.; Wong, K.; Ng, M. ; et al. Source apportionment of fine particulate matter in Macao, China with and without organic tracers: A comparative study using positive matrix factorization. *Atmos. Environ*. **2019**. 198, 183-193.
12. Schauer, J.J.; Kleeman, M.J.; Cass, G.R.; Simoneit, B.R.T. Measurement of emissions from air pollution sources. 4. C1− C27 organic compounds from cooking with seed oils. *Environ. Sci. Technol.* **2002**. 36, 567-575.
13. Gadi, R.; Shivani; Sharma, S.K.; Mandal, T.K. Source apportionment and health risk assessment of organic constituents in fine ambient aerosols (PM2. 5): A complete year study over National Capital Region of India. *Chemos*. **2019**. 221, 583-596.
14. Zhao, Y.; Hennigan, C.J.; May, A.A.; Tkacik, D.S.; de Gouw, J.A.; Gilman, J.B.; Kuster, W.C.; Borbon, A.; Robinson, A.L. Intermediate-Volatility Organic Compounds: A Large Source of Secondary Organic Aerosol. *Environ. Sci. Technol*. **2014**. 48, 13743–13750.
15. Aumont, B.; Valorso, R.; Mouchel-Vallon, C.; Camredon, M.; Lee-Taylor, J.; Madronich, S. Modeling SOA formation from the oxidation of intermediate volatility n-alkanes. *Atmos. Chem. Phys*. **2012**. 12, 7577-7589.
16. Chan, A.W.H.; Kautzman, K.E.; Chhabra, P.S.; Surratt, J.D.; Chan, M.N.; Crounse, J.D.; Kürten, A.; Wennberg, P.O.; Flagan, R.C.; Seinfeld, J.H. Secondary organic aerosol formation from photooxidation of naphthalene and alkylnaphthalenes: Implications for oxidation of intermediate volatility organic compounds (IVOCs). *Atmos. Chem. Phys*. **2009**, 9, 3049–3060.
17. Zhao, Y.; Nguyen, N.T.; Presto, A.A.; Hennigan, C.J.; May, A.; Robinson, A. Intermediate Volatility Organic Compound Emissions from On-Road Gasoline Vehicles and Small Off-Road Gasoline *Engines. Environ. Sci. Technol*. **2016**, 50, 4554–4563.
18. Brown, S.G. Eberly, S.; Paatero, P.; Norris, G.A. Methods for estimating uncertainty in PMF solutions: examples with ambient air and water quality data and guidance on reporting PMF results. *Sci. Total. Environ.* **2015**. 518-519, 626-35.
19. Qian, Z.; Chen, J.; Liu, Y.; Han, Y.; Zhang, S.; Feng, L.; Shang, Y.; Guo, H.; Li, Q.; Shen, F.; et al. Intermediate Volatile Organic Compound Emissions from Residential Solid Fuel Combustion Based on Field Measurements in Rural China. *Environ. Sci. Technol*. **2021**, 55, 5689–5700.